HHS Public Access

Author manuscript

J Am Chem Soc. Author manuscript; available in PMC 2020 January 30.

Published in final edited form as:

J Am Chem Soc. 2019 January 30; 141(4): 1415–1419. doi:10.1021/jacs.8b09769.

Nitrosyl Linkage Isomers: NO Coupling to N_2O at a Mononuclear Site

Subrata Kundu[†,‡], **Phan N. Phu**[§], **Pokhraj Ghosh**[†], **Stosh A. Kozimor**[‖], **Jeffery A. Bertke**[†], **S. Chantal E. Stieber**[*,§,‖], **Timothy H. Warren**[*,†]

[†] Department of Chemistry, Georgetown University, Box 571227-1227, Washington, D. C. 20057, United States

[‡] School of Chemistry, Indian Institute of Science Education and Research Thiruvananthapuram, Kerala 695551, India

[§] California State Polytechnic University, Pomona, California 91768, United States

[‖] Los Alamos National Laboratory, MS K558, Los Alamos, New Mexico 87545, United States

Abstract

Linkage isomers of reduced metal-nitrosyl complexes serve as key species in nitric oxide (NO) reduction at monometallic sites to produce nitrous oxide (N_2O), a potent greenhouse gas. While factors leading to extremely rare side-on nitrosyls are unclear, we describe a pair of nickel-nitrosyl linkage isomers through controlled tuning of noncovalent interactions between the nitrosyl ligands and differently encapsulated potassium cations. Furthermore, these reduced metal-nitrosyl species with N-centered spin density undergo radical coupling with free NO and provide a N–N coupled *cis*-hyponitrite intermediate whose protonation triggers the release of N_2O. This report outlines a stepwise molecular mechanism of NO reduction to form N_2O at a mononuclear metal site that provides insight into the related biological reduction of NO to N_2O.

Nitrous oxide (N_2O) is a long-lived (ca. 114 years) greenhouse gas with a global warming potential 298 times that of CO_2 on a molecular basis.[1] Enhanced through feeding of crops with nitrogen-rich fertilizers,[2] global emission of N_2O is mainly attributed to the microbial and fungal denitrification processes mediated by metalloenzymes.[3] The most critical step for N_2O generation is N–N bond formation that occurs via the reductive coupling of two nitric

[*]**Corresponding Authors** thw@georgetown.edu, sestieber@cpp.edu.

The authors declare no competing financial interest.

ASSOCIATED CONTENT

Supporting Information

The Supporting Information is available free of charge on the ACS Publications website at DOI: 10.1021/jacs.8b09769.

Experimental, characterization, and computational details (PDF)

X-ray crystallographic data of **1** (CIF)

X-ray crystallographic data of **2a** (CIF)

X-ray crystallographic data of **2b** (CIF)

X-ray crystallographic data of **3a** (CIF)

X-ray crystallographic data of **3b** (CIF)

X-ray crystallographic data of **4** (CIF)

NOTE ADDED IN PROOF

Coupling of NO at a dinickel complex to form a dinuclear cis-hyponitrite has been reported while this manuscript was under review.[29]

oxide (NO) molecules. This takes place at diiron sites of nitric oxide reductase (NOR) enzymes[4] as well as at mononuclear sites in the iron-based cytochrome P450 nitric oxide reductase (NOR)[5] or copper nitrite reductase (CuNiR)[6] enzymes (Figure 1a). Based on numerous theoretical studies, it seems likely that an intermediate hyponitrite species ($N_2O_2^{2-}$) precedes N_2O release.[7] For instance, coupling of two metal-nitrosyl [M]-NO moieties takes place upon reduction of $[(TpRuNO)_2(\mu\text{-}Cl)(\mu\text{-}Pz)]^{2+}$ to afford the N–N reductively coupled product $(TpRu)_2(\mu\text{-}Cl)(\mu\text{-}Pz)\{\mu\text{-}\kappa^2\text{-}N(=O)N(=O)\}$.[8] Reductive coupling of NO at copper(I) complexes has led to dinuclear *trans*-hyponitrite copper(II) complexes $[Cu^{II}]_2(\mu\text{-}O_2N_2)$ that release N_2O either upon acidification[9] or thermal decay;[10] the later also produces $[Cu^{II}](NO_2)$ via disproportionation.[10] The nickel nitrosyl $[(bipy)(Me_2phen)NiNO][PF_6]$ mediates NO disproportionation in the presence of NO and yields N_2O via a mononuclear *cis*-hyponitrite $[Ni](\kappa^2\text{-}O_2N_2)$.[11] The factors that lead to N–N bond formation at a monometallic site, however, have not been explicitly documented.[12]

We hypothesize that the presence of spin density at the N atom of a metal-nitrosyl [M]-NO, perhaps enhanced by the ability to achieve a side-on [M]-NO conformation, may facilitate N–N bond formation between a metal-nitrosyl and nitric oxide to give *cis*-hyponitrites $[M](\kappa^2\text{-}O_2N_2)$ (Figure 1e). Access to side-on $[M](\eta^2\text{-NO})$ complexes may both expose the N atom for N–N coupling and initiate a M-O interaction prior to forming mononuclear $[M](\kappa^2\text{-}O_2N_2)$ complexes. Such side-on conformations are known in the photoexcited states of $\{Ni(NO)\}^{10}$ complexes[13] where the superscript in the Enemark–Feltham formulation $\{Ni(NO)\}^{10}$ represents the total number of metal d and NO π^* electrons.[14] The side-on binding of a nitrosyl ligand (Figure 1d) in a mononuclear synthetic complex, however, has not been observed in its ground state. $\{[(Me_3Si)_2N]_2(THF)Y\}_2(\mu\text{-}\eta^2\text{:}\eta^2\text{-NO})$ is a singular example that possesses a side-on NO achieved via bridging between two transition or rare earth metal centers that possesses a highly reduced NO^{2-} ligand.[15] Crystallographic studies revealed side-on η^2-NO binding in fully reduced bovine cytochrome c oxidase (CcO)[16] and copper nitrite reductase (CuNiR)[17] that feature mononuclear $\{Cu\text{-}(NO)\}^{11}$ sites, though solution spectroscopic studies suggest end-on binding.[18,19] DFT calculations for both side-on and end-on $\{Cu(NO)\}^{11}$ species suggest that each possesses a $Cu^{I}(\cdot NO)$ electronic formulation[20] with a considerable amount of spin density at the nitrosyl N atom, reinforced by EPR studies of the reduced $\{Cu(NO)\}^{11}$ intermediate of CuNIR.[18,21] Furthermore, differential H-bonding and/or steric interactions from second-sphere protein residues may play a vital role in the determining the conformation of $\{Cu(NO)\}^{11}$ species.[21,22]

To synthetically outline factors that control metal-nitrosyl bonding modes and NO coupling reactivity, we targeted low coordinate $\{M(NO)\}^{10/11}$ pairs that could accommodate both side-on NO and *cis*-hyponitrite ligands (Figure 1d,e). The salt metathesis reaction between equimolar amounts of the β-diketiminato potassium salt $[^{i}Pr_2NN_{F6}]K(THF)$ and $(THF)_2Ni(NO)I$ in tetrahydrofuran (THF) affords the diamagnetic $\{Ni(NO)\}^{10}$ complex $[^{i}Pr_2NN_{F6}]NiNO$ (**1**) isolated as dark green crystals in 76% yield (Figure 2a). The X-ray structure of **1** reveals a trigonal-planar Ni center with an end-on nitrosyl ligand (Nil–N3–O1 = 174.47(11)°) with a N3–O1 distance of 1.1602(15) Å (Figure S22). The infrared spectrum of **1** indicates a nitrosyl stretch ((ν_{NO}) at 1825 cm^{-1}, similar to values reported for other three-coordinate neutral nickel-nitrosyl complexes (ν_{NO} = 1817–1779 cm^{-1}).[23] Notably, the

cyclic voltammogram of **1** in tetrahydrofuran at room temperature exhibits a reversible reduction wave centered at −1.89 V (vs ferrocenium/ferrocene), attributed to the $\{Ni(NO)\}^{10/11}$ redox couple (Figure S6).

One-electron reduction of the $\{Ni(NO)\}^{10}$ complex **1** with potassium-graphite (KC_8) (1.2 equiv) in tetrahydrofuran in the presence of 18-crown-6 (1 equiv) leads to a rapid color change from green to purple (Figure 2a). Single crystal X-ray diffraction analysis of the purple complex **2a** reveals two independent $[^{i}Pr_2NN_{F6}]Ni(\mu\text{-}\eta^2\text{:}\ \eta^2\text{-NO})K(18\text{-crown-6})(THF)$ moieties. Each nickel exhibits square planar coordination that features a side-on NO ligand between the Ni and K centers. Although disorder from interchange of N/O positions precludes a detailed assessment of metrical parameters, refinement of the NO ligand into a single orientation (Figure 2b) gives short Ni–N (1.853(5) Å; 1.866(5) Å) and Ni–O (1.839(5) Å; 1.868(5) Å) distances similar to those observed in a related [Ni](η^2-ONPh) complex.[24] The nitrosyl ligand in the $\{Ni(NO)\}^{11}$ species **2a** (molecule 1: 1.270(6) Å; molecule 2: 1.284(6) Å) is significantly more activated than in the $\{Ni(NO)\}^{10}$ analogue **1** (1.1602(15) Å), despite N/O positional disorder that likely underestimates the N–O distance.[15] Disorder models that allow pairs of N/O atoms to refine lead to slightly longer N–O distances of 1.28–1.32 Å but with a wider spread of Ni–N/O distances (Figure S23c,d). Thus, **2a** possesses a nitrosyl ligand with a N–O distance longer than in most metal-nitrosyls[25] except $\{[(Me_3Si)_2N]_2(THF)Y\}_2$(,M-$\eta^2\text{:}\eta^2$-NO), which also features a side-on NO ligand (N–O: 1.390(4)Å).[15] Coordination of the potassium cation to both the nitrogen and oxygen atoms of the reduced nitrosyl ligand in the $\{[Ni](\eta^2\text{-NO})\}^{-}$ anion of **2a** gives K–N/O distances in the range 2.826(5) Å - 2.869(5) Å that leads to Ni···K separations of 4.417 Å (molecule 1) and 4.467 Å (molecule 2). The infrared spectra of two isotopologues **2a** and **2a**-^{15}N exhibit $^{14}N/^{15}N$ isotope sensitive bands at 894 and 878 cm^{-1}, respectively. This is the lowest ν_{NO} reported for a transition metal nitrosyl complex, lower than 951 cm^{-1} in $\{[(Me_3Si)_2N]_2(THF)Y\}_2(\mu\text{-}\eta^2\text{:}\eta^2\text{-NO})$.[15]

More completely encapusulating the K^+ cation changes the nitrosyl bonding mode of the $\{[Ni](NO)\}^{-}$ anion. Reduction of $[^{i}Pr_2NN_{F6}]NiNO$ (**1**) with KC_8 (1.2 equiv) in the presence of [2.2.2]-cryptand (1 equiv) in tetrahydrofuran gives $[^{i}Pr_2NN_{F6}]Ni(\mu\text{-NO})K$[2.2.2-cryptand] (**2b**) (Figures 2c, S24). By significantly lengthening the Ni···K separation (5.466 Å), the nitrosyl ligand exhibits both linear (77%) and side-on (23%) conformations in the solid state. The linear NO ligand (Ni1–N3A–O1A, 165.8(3)°) in **2b** is more highly reduced than in **1** with a N–O distance of 1.198(4) Å. The minor side-on conformer exhibits N/O positional disorder whose principle component possesses a N–O distance of 1.274(19) Å similar to **2a**. The IR spectrum of a solid sample of **2b** reveals an NO stretch at 1555 cm^{-1} (1525 cm^{-1} for **2b**-^{15}NO) that is consistent with a highly reduced linear NO ligand (Figure S10).[25]

The room temperature EPR spectrum of $[^{i}Pr_2NN_{F6}]Ni(\mu\text{-}\eta^2\text{:}\eta^2\text{-NO})K$[18-crown-6](THF) (**2a**) in tetrahydrofuran indicates a $S = 1/2$ species with a g_{iso} value of 2.0008, very close to that of the free electron (g_e = 2.0023). This three line spectrum of **2a** is due to strong coupling with the ^{14}N nucleus of the bound NO ligand (A_{14N} = 28.9 MHz), which shifts to a two line pattern for **2a**-^{15}N (A_{15N} = 40.1 MHz) (Figure 3a,b). These data are very similar to the highly reduced, radical NO^{2-} dianion in $\{[(Me_3Si)_2N]_2(THF)Y\}_2(\mu\text{-}\eta^2\text{:}\eta^2\text{-NO})$.[15] In both THF solution and frozen glass (20 K), EPR spectra of **2a** and **2b** are nearly

indistinguishable (Figures S20 and S21). Modeling of the low T EPR spectra of **2a** was guided by DFT calculations and required the use of two separate components, suggesting that THF solutions of **2a** and **2b** may contain a mixture of side-on and linear nitrosyls.

Ni K-edge X-ray absorption spectroscopy (XAS) probes the Ni oxidation state by exciting a Ni 1s electron to valence Ni 3d orbitals (pre-edge, ~8330–8335 eV) and Ni 4p orbitals (edge, >8345 eV) (Figure 3c). The pre-edge features of **1** (8332.1(0) eV), **2a** (8332.3(1) eV), and **2b** (8332.3(0) eV) are at a similar energy to the closely related Ni^{II} complex $[^{i}Pr_2NN_{F6}]Ni^{II}(\mu\text{-}Br)_2Li(THF)_2$, (8331.6 eV),[24] suggesting that complexes **1**, **2a**, and **2b** are best described as Ni^{II}, with the slight shift to higher pre-edge energies attributed to NO backbonding. Calculated TDDFT XAS assign the rising edge feature in **2a** and **2b** at ~8335 eV is a Ni to ligand π^*transition that has much weaker intensity in **1** (Figure S38). These results suggest that reduction of $\{Ni(NO)\}^{10}$ species **1** to anionic $\{Ni(NO)\}^{11}$ species **2a** and **2b** occurs primarily at the NO ligand. Complexes **2a** (side-on) and **2b** (principally end-on) have nearly identical XAS spectra and cannot be readily distinguished by this technique.

DFT calculations (Supporting Information) provide insight into electronic structure of the NO complexes and the secondary sphere interactions that control the NO bonding mode. DFT geometry optimizations of **1**, **2a**, and **2b** without counterions using the ORCA program[26] (B3LYP, TZVP/SV(P)) reveal spin density at the NO ligand in the **2a** side-on (1.25 e^-) and **2b** end-on conformations (1.52 e^-) that are almost identical in energy. Similar to TpNiNO with a linear NO ligand,[27] complex **1** is best described as high spin Ni(II) antiferromagnetically coupled to NO^{1-} while the anionic complexes **2a** and **2b** are low spin Ni(II) with an NO^{2-} ligand (Figures S33 and S35). Full molecule calculations could energetically distinguish the end-on and side on conformations by fixing the Ni···K distance to 5.466 Å. This revealed the side-on conformation to be only 2.3 kcal/mol more stable, consistent with the linear/side-on disordered observed in the solid state structure of **2b**.

The reduced NO ligands that bear significant unpaired electron density in **2a** and **2b** are primed for coupling with •NO to form *cis*-hyponitrite ligands in complexes $\{[Ni](\kappa^2\text{-}O_2N_2)\}^-$ (**3a** and **3b**). Addition of 1 equiv $NO_{(g)}$ to **2a** in tetrahydrofuran at room temperature affords diamagnetic $\{[^{i}Pr_2NN_{F6}]Ni(\kappa^2\text{-}O_2N_2)\}K(18\text{-crown-6})$ (**3a**) in 72% yield (Figure 4a). X-ray diffraction analysis of **3a** reveals a square planar Ni center with short $Ni\text{–}N_{\beta\text{-dik}}$ 1.8895(15), 1.8936(15) Å and Ni–O 1.8241(13), 1.8187(13) Å) distances clearly indicating coupling between the two NO ligands (N3–N4 = 1.235(2) Å) (Figures 4b and S25). The *cis*-hyponitrite ligand exhibits an otherwise symmetric structure (O1–N3 = 1.370(2), O2–N4 = 1.367(2) Å) similar to those previously observed[12] despite unsymmetrical coordination of $\{K[18\text{-crown-6}]\}^+$ cation to both the N atoms of the hyponitrite ligand (K1–N4, 2.7519(17), K1–N3, 3.0584(18) Å). Addition of NO to **2b** similarly provides $\{[^{i}Pr_2NN_{F6}]Ni(\kappa^2\text{-}O_2N_2)\}K[2.2.2\text{-cryptand}]$ (**3b**) in 89% yield with very similar metrical parameters for the $\{[Ni](\kappa^2\text{-}O_2N_2)\}^-$ moiety that is coordinated to only one *cis*-hyponitrite N atom by the $\{K[2.2.2\text{-cryptand}]\}^+$ cation (K–N = 3.274 Å) (Figure S26). Capture of NO by a reduced NO ligand in $\{[Ni](NO)\}^-$ to form *cis*-hyponitrites $\{[Ni](\kappa^2\text{-}O_2N_2)\}^-$ mirrors the reactivity of NO with $[^{i}Pr_2NN_{F6}]Ni(\eta^2\text{-ONPh})$ to form $[^{i}Pr_2NN_{F6}]Ni\text{-}(\eta^2\text{-}O_2N_2Ph)$. In both anionic $\{[Ni](NO)\}^-$ and neutral $[Ni](\eta^2\text{-ONPh})$, there is significant

unpaired electron density at the reduced NO moiety.[24] Notably, the $\{Ni(NO)\}^{10}$ complex **1** does not react with nitric oxide.

NMR spectra of $\{[^{i}Pr_2NN_{F6}]Ni(\kappa^2\text{-}O_2N_2)\}K[18\text{-crown-6}]$ (**3a**) in THF-d_8 exhibits sharp resonances characteristic of diamagnetic β-diketiminato Ni^{II} complexes (Figures S12–S14).[24] Notably, the ^{15}N NMR spectrum of a ^{15}N enriched sample of **3a** (**3a**-$^{15}N^{15}N$) in THF-d_8 shows a sharp singlet at 244.7 ppm (vs liquid NH_3) indicating symmetric κ^2-*O,O* binding of the hyponitrite ligand to the $[^{i}Pr_2NN_{F6}]Ni$ core in solution at room temperature. The $\{[^{i}Pr_2NN_{F6}]Ni(\kappa^2\text{-}O_2N_2)\}^{-}$ anion in **3b** exhibits identical NMR features as found in **3a**.

Hyponitrite complexes are known to release N_2O upon heating or protonation.[9,10,12] The $\{[^{i}Pr_2NN_{F6}]Ni(\kappa^2\text{-}O_2N_2)\}^{-}$ anion (in **3a** or **3b**) is thermally stable up to 60 °C with no evidence of N_2O loss. Protonation of **3a** or **3b** by 1 equiv trifluoroacetic acid, however, triggers the instantaneous release of N_2O observed by ^{15}N NMR (Figures 4c and S17) and IR spectroscopy (2227 cm^{-1}) (Figure S16). Protonation with $HBF_4{\cdot}OEt_2$ produces N_2O in 76% yield and allows for isolation of the nickel(II) hydroxide dimer $\{[^{i}Pr_2NN_{F6}]Ni\}_2(\mu\text{-}OH)_2$ (**4**) in 66% yield that exhibits a structure similar to other β-diketiminato $[Ni^{II}]_2(\mu\text{-}OH)_2$ complexes (Figure S27).[28]

Spectroscopic and computational insights reveal that one-electron reduction of the $\{Ni(NO)\}^{10}$ complex **1** largely takes place at the NO ligand, leading to side-on and end-on $\{Ni(NO)\}^{11}$ species **2a** and **2b**, respectively. Regardless of the nitrosyl binding mode, these $\{Ni(NO)\}^{11}$ complexes possess a significant amount of unpaired electron density at the nitrosyl N atom and undergo facile coupling with NO to give the *cis*-hyponitrite $\{[Ni](\kappa^2\text{-}O_2N_2)\}^{-}$, which releases N_2O upon protonation. Controlled tuning of the second coordination sphere interactions between the nitrosyl ligand of the $\{Ni(NO)\}^{11}$ anion and a potassium cation modifies the metal-nitrosyl bonding mode, favoring side-on $[M](\eta^2\text{-}NO)$ at shorter Ni···K distances. Especially because the corresponding $\{Ni(NO)\}^{10}$ species does not react with NO, these findings underscore electronic and conformational factors that favor NO coupling via N–N bond formation at monometallic sites. Separation of NO-based reduction and NO coupling steps provides important context for the biologically important reduction of NO that results in N_2O formation via protonation of *cis*-hyponitrite intermediates.

Supplementary Material

Refer to Web version on PubMed Central for supplementary material.

ACKNOWLEDGMENTS

T.H.W. acknowledges the NSF (CHE-1459090), the NIH (R01GM126205), and the Georgetown Environment Initiative. S.C.E.S. acknowledges the CPP College of Science, a CSUPERB New Investigator Grant, and NSF XSEDE (CHE160059). S.A.K. acknowledges the Heavy Element Chemistry Program by the Division of Chemical Sciences, Geosciences, and Biosciences, Office of Basic Energy Sciences (BES), U.S. Department of Energy, and Seaborg Institute Postdoctoral Fellowship (S.C.E.S.). LANL is operated by Los Alamos National Security, LLC, for the National Nuclear Security Administration of U.S. DOE (DE-AC52-06NA25396). Use of Stanford Synchrotron Radiation Light source, SLAC National Accelerator Laboratory, supported by DOE, Office of Science, BES (DE-AC02-76SF00515).

REFERENCES

(1). Ravishankara AR; Daniel JS; Portmann RW Nitrous Oxide (N2O): The Dominant Ozone-Depleting Substance Emitted in the 21st Century. Science 2009, 326, 123–125. [PubMed: 19713491]

(2). Reay DS; Davidson EA; Smith KA; Smith P; Melillo JM; Dentener F; Crutzen PJ Global agriculture and nitrous oxide emissions. Nat. Clim. Change 2012, 2, 410–416.

(3). Thomson AJ; Giannopoulos G; Pretty J; Baggs EM; Richardson DJ Biological sources and sinks of nitrous oxide and strategies to mitigate emissions. Philos. Trans. R Soc., B 2012, 367, 1157–1168.

(4). Shiro Y; Sugimoto H; Tosha T; Nagano S; Hino T Structural Basis for Nitrous Oxide Generation by Bacterial Nitric Oxide Reductases. Philos. Trans. R. Soc., B 2012, 367, 1195–1203.

(5). McQuarters AB; Wirgau NE; Lehnert N Model Complexes of Key Intermediates in Fungal Cytochrome P450 Nitric Oxide Reductase (P450nor). Curr. Opin. Chem. Biol 2014, 19, 82–89. [PubMed: 24658055]

(6). Merkle AC; Lehnert N Binding and Activation of Nitrite and Nitric Oxide by Copper Nitrite Reductase and Corresponding Model Complexes. Dalton Trans 2012, 41, 3355–3368. [PubMed: 21918782]

(7). (a)Blomberg MRA; Siegbahn PEM Mechanism for N_2O Generation in Bacterial Nitric Oxide Reductase: A Quantum Chemical Study. Biochemistry 2012, 51, 5173–5186. [PubMed: 22680334] (b)Metz S N_2O Formation via Reductive Disproportionation of NO by Mononuclear Copper Complexes: A Mechanistic DFT Study. Inorg. Chem 2017, 56, 3820–3833. [PubMed: 28291346] (c)Suzuki T; Tanaka H; Shiota Y; Sajith PK; Arikawa Y; Yoshizawa K Proton-Assisted Mechanism of NO Reduction on a Dinuclear Ruthenium Complex. Inorg. Chem 2015, 54, 7181–7191. [PubMed: 26186365]

(8). Arikawa Y; Asayama T; Moriguchi Y; Agari S; Onishi M Reversible N-N Coupling of NO Ligands on Dinuclear Ruthenium Complexes and Subsequent N_2O Evolution: Relevance to Nitric Oxide Reductase. J. Am. Chem. Soc 2007, 129, 14160–14161. [PubMed: 17973393]

(9). Lionetti D; de Ruiter G; Agapie T A Trans-Hyponitrite Intermediate in the Reductive Coupling and Deoxygenation of Nitric Oxide by a Tricopper-Lewis Acid Complex. J. Am. Chem. Soc 2016, 138, 5008–5011. [PubMed: 27028157]

(10). Wijeratne GB; Hematian S; Siegler MA; Karlin KD Copper(I)/NO(g)Reductive Coupling Producing a Trans-Hyponitrite Bridged Dicopper(II) Complex: Redox Reversal Giving Copper-(I)/NO(g)Disproportionation. J. Am. Chem. Soc 2017, 139, 13276–13279. [PubMed: 28820592]

(11). Wright AM; Zaman HT; Wu G; Hayton TW Mechanistic Insights into the Formation of N_2O by a Nickel Nitrosyl Complex. Inorg. Chem 2014, 53, 3108–3116. [PubMed: 24597563]

(12). (a)Wright AM; Hayton TW Understanding the Role of Hyponitrite in Nitric Oxide Reduction. Inorg. Chem 2015, 54, 9330–9341. [PubMed: 25928662] (b)Arikawa Y; Onishi M Reductive N-N Coupling of NO Molecules on Transition Metal Complexes Leading to N_2O. Coord. Chem. Rev 2012, 256, 468–478.

(13). Fomitchev DV; Furlani TR; Coppens P Combined X-Ray Diffraction and Density Functional Study of [Ni(NO)(η5-Cp*)] in the Ground and Light-Induced Metastable States. Inorg. Chem 1998, 37, 1519–1526.

(14). Enemark JH; Feltham RD Principles of Structure, Bonding, and Reactivity for Metal Nitrosyl Complexes. Coord. Chem. Rev 1974, 13, 339–406.

(15). Evans WJ; Fang M; Bates JE; Furche F; Ziller JW; Kiesz MD; Zink JI Isolation of a radical dianion of nitrogen oxide (NO)2−. Nat. Chem 2010, 2, 644–647. [PubMed: 20651726]

(16). Ohta K; Muramoto K; Shinzawa-Itoh K; Yamashita E; Yoshikawa S; Tsukihara T X-Ray Structure of the NO-Bound CuB in Bovine Cytochrome c Oxidase. Acta Crystallogr., Sect. F: Struct. Biol. Cryst. Commun 2010, 66, 251–253.

(17). Tocheva EI; Rosell FI; Mauk AG; Murphy MEP Side-on Copper-Nitrosyl Coordination by Nitrite Reductase. Science 2004, 304, 867–870. [PubMed: 15131305]

(18). Usov OM; Sun Y; Grigoryants VM; Shapleigh JP; Scholes CP EPR-ENDOR of the Cu(I)NO Complex of Nitrite Reductase. J. Am. Chem. Soc 2006, 128, 13102–13111. [PubMed: 17017790]

(19). Fujisawa K; Tateda A; Miyashita Y; Okamoto K; Paulat F; Praneeth VKK; Merkle A; Lehnert N Structural and Spectroscopic Characterization of Mononuclear copper(I) Nitrosyl Complexes: End-on versus Side-on Coordination of NO to copper(I). J. Am. Chem. Soc 2008, 130, 1205–1213. [PubMed: 18179210]

(20). Wasbotten IH; Ghosh A Modeling Side-on NO Coordination to Type 2 Copper in Nitrite Reductase: Structures, Energetics, and Bonding. J. Am. Chem. Soc 2005, 127, 15384–15385. [PubMed: 16262398]

(21). Ghosh S; Dey A; Usov OM; Sun Y; Grigoryants VM; Scholes CP; Solomon EI Resolution of the Spectroscopy versus Crystallography Issue for NO Intermediates of Nitrite Reductase from Rhodobacter Sphaeroides. J. Am. Chem. Soc 2007, 129, 10310–10311. [PubMed: 17685522]

(22). Merkle AC; Lehnert N The Side-on Copper(I) Nitrosyl Geometry in Copper Nitrite Reductase Is Due to Steric Interactions with Isoleucine-257. Inorg. Chem 2009, 48, 11504–11506. [PubMed: 19938869]

(23). Puiu SC; Warren TH Three-Coordinate-Diketiminato Nickel Nitrosyl Complexes from Nickel(I)-Lutidine and Nickel(II) - Alkyl Precursors. Organometallics 2003, 22, 3974–3976.

(24). Kundu S; Stieber SCE; Ferrier MG; Kozimor SA; Bertke JA; Warren TH Redox Non-Innocence of Nitrosobenzene at Nickel. Angew. Chem., Int. Ed 2016, 55, 10321–10325.

(25). (a)Hayton TW; Legzdins P; Sharp WB Coordination and Organometallic Chemistry of Metal-NO Complexes. Chem. Rev 2002, 102, 935–991. [PubMed: 11942784] (b)Böhmer J; Haselhorst G; Wieghardt K; Nuber B The First Mononuclear Nitrosyl(oxo)molybdenum Complex: Side-On Bonded and μ3-bridging NO Ligands in [{MoL(NO)(O)-(OH)}2NaPF6·H2O. Angew. Chem., Int. Ed. Engl 1994, 33, 14731476.

(26). Neese F Orca: an ab initio, DFT and Semiempirical Electronic Structure Package, Version 3.0.3; Max Planck Institute for Chemical Energy Conversion: Mulheim an der Ruhr, Germany.

(27). (a)Tomson NC; Crimmin MR; Petrenko T; Rosebrugh LE; Sproules S; Boyd WC; Bergman RG; Debeer S; Toste FD; Wieghardt K A Step Beyond the Feltham-Enenark Notation: Spectroscopic and Correlated ab Initio Computational Support for an Antiferromagnetically Coupled M(II)-(NO)− Description of Tp*M-(NO)(M = Co, Ni). J. Am. Chem. Soc 2011, 133, 18785–18801." [PubMed: 22047035] (b)Soma S; Van Stappen C; Kiss M; Szilagyi RK; Lehnert M; Fujisawa K Distorted tetrahedral nickel-nitrosyl complexes: spectroscopic characterization and electronic structure. J. Biol. Inorg. Chem 2016, 21, 757–775. [PubMed: 27350153]

(28). Yao S; Bill E; Milsmann C; Wieghardt K; Driess MA "Side-on" superoxonickel Complex [LNi(O2)] with a Square-Planar Tetracoordinate Nickel(II) Center and Its Conversion into [LNi(μ-OH)2NiL]. Angew. Chem., Int. Ed 2008, 47, 7110–7113.

(29). Ferretti E; Dechert S; Demeshko S; Holthausen MC; Meyer F Reductive Nitric Oxide Coupling at a Dinickel Core: Isolation of a Key cis-Hyponitrite Intermediate en route to N_2O Formation. Angew. Chem. Int. Ed 2019, DOI: 10.1002/anie.201811925.

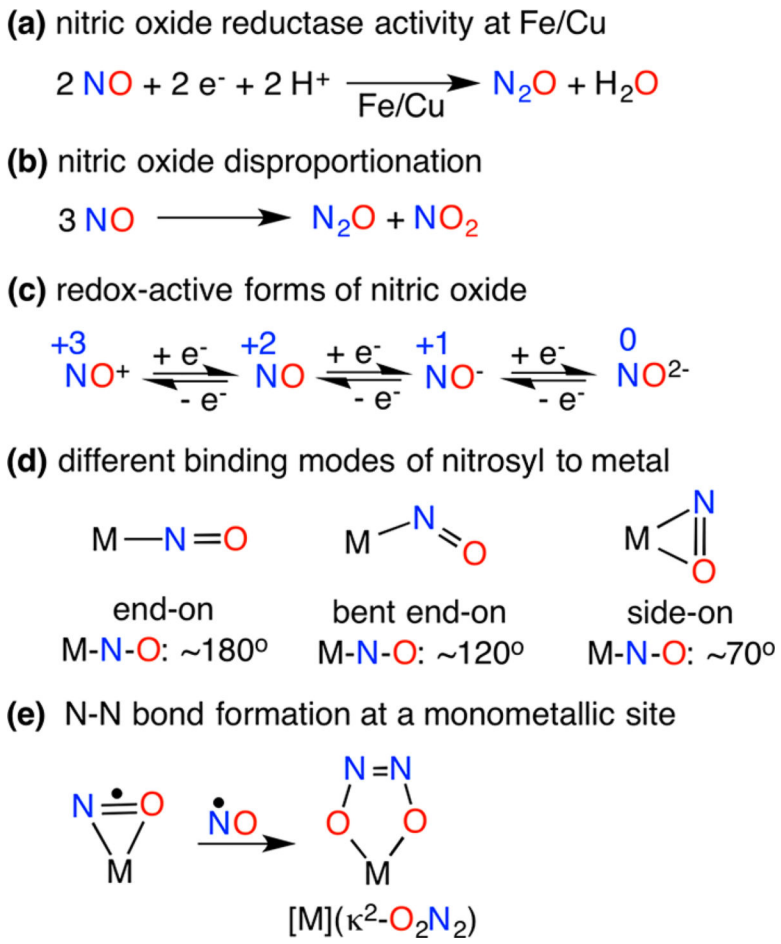

Figure 1.
Reactivity and binding of nitrosyl ligands at transition metal sites.

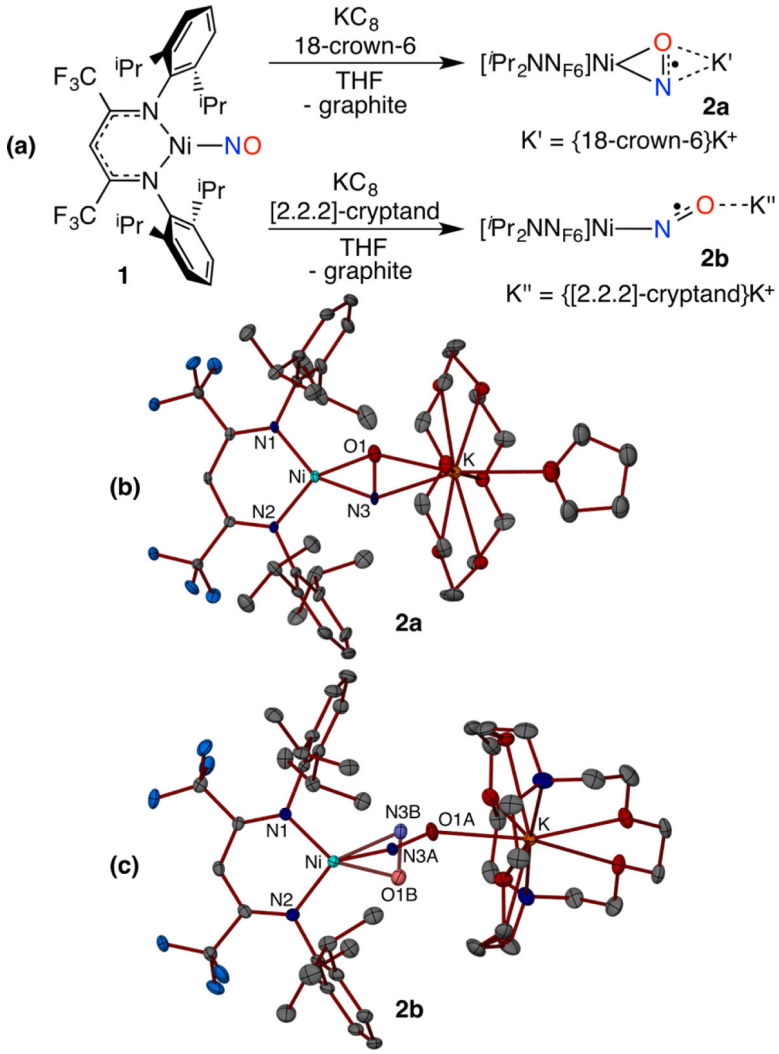

Figure 2.

Synthesis (a) and X-ray structures (b,c) of $\{NiNO\}^{11}$ anions **2a** (side-on) and **2b** (77/23 end-on/side-on).

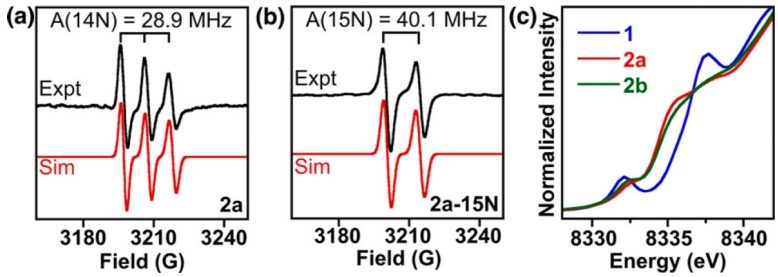

Figure 3.

(a, b) X-band EPR spectra (black trace) of **2a** and **2a**-^{15}N in tetrahydrofuran at 293 K. Simulations (red trace) provide g_{iso} = 2.0008, A_{iso}(^{14}N) = 28.9 MHz (for **2a**), and A_{iso}(^{15}N) = 40.1 MHz (for **2a**-^{15}N). (c) Ni K-edge X-ray absorption spectra of **1**, **2a**, and **2b**.

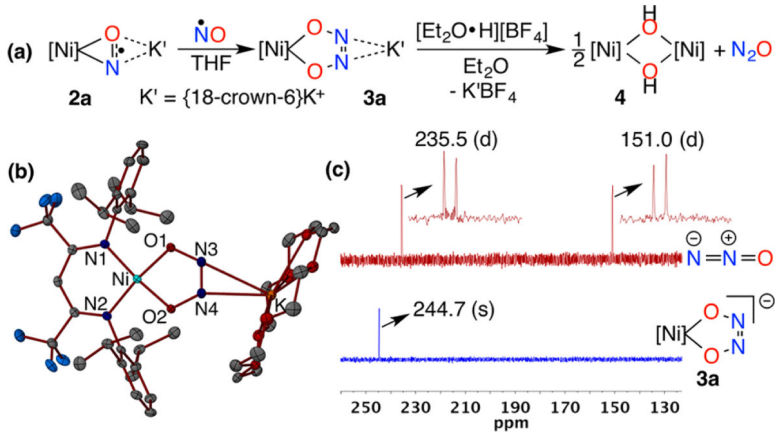

Figure 4.

(a) Formation of *cis*-hyponitrite intermediate **3a** and its transformation to nitrous oxide. (b) X-ray crystal structure of **3a**. (c) Comparison of ^{15}N NMR spectra (41 MHz, 298 K, tetrahydrofuran-d_8) of [Ni](κ^2-$O_2{}^{15}N_2$)K[18-crown-6] (**3a**-$^{15}N^{15}N$) (blue trace) and the crude reaction mixture (red trace) obtained upon addition of 1 equiv trifluoroacetic acid to a solution of **3a**-$^{15}N^{15}N$ in tetrahydrofuran-d_8.